Divergence instabilities of non-uniformly pre-stressed travelling webs

Ciprian D. Coman[†]

School of Computing & Engineering,
University of Huddersfield, HD1 3DH, Huddersfield, UK

November 24, 2023

Abstract

The phenomenon of edge-buckling in an axially moving stretched thin elastic web is described as a non-standard singularly-perturbed bifurcation problem, which is then explored through the application of matched asymptotic techniques. Previous numerical work recently reported in the literature is re-evaluated in this context by approaching it through the lens of asymptotic simplifications. This allows us to identify two distinct regimes characterised by qualitative differences in the corresponding eigen-deformations; some simple approximate formulae for the critical eigenvalues are also proposed. The obtained analytical results capture the intricate relationship between the critical speeds, the background tension, and other relevant physical and geometric parameters that feature in the mathematical model.

Keywords: axial motions; buckling; boundary layers; thin-plate theory; matched asymptotics.

[†] `cdc3p@yahoo.com`

1 Introduction

Axially moving webs (AMWs) hold significant importance in various industrial contexts due to their wide range of uses and benefits. They play a crucial role in continuously manufacturing processes, enabling the efficient production of materials like paper, plastic films, textiles, and metal sheets. AMWs also facilitate precise coating, printing, as well as mechanical or chemical treatment processes. The ability to transport webs at high speeds and control their motions results in increased productivity. Nevertheless, there are several unique factors that limit the operational speeds employed in these types of applications; the mechanical instability of the web is one them.

A common form of instability observed in both moving and stationary webs (as well as in thin strips) is *wrinkling*; this occurs when the web undergoes local compressive forces, causing it to buckle or fold. The presence of compression in a configuration that is normally designed to operate under uniaxial tension is somewhat counter-intuitive, and it is essentially connected to the free edges of the web. While the normal and shear stress components are zero on such edges, away from them the stress state can become compressive and thus wrinkles might develop (e.g., [1, 2, 3, 4]). There are several possible factors associated with the compressive forces mentioned above. For example, in metal forming applications residual stresses are known to have a detrimental effect that could be responsible for the buckling instabilities frequently encountered in rolling and levelling processes (e.g., see [5, 6, 7] and the references therein). The misalignment of the rollers that support the moving web (and over which it passes) can also play a destabilising role. If such rollers are co-planar but not parallel to each other, the tractions they impart to the web may no longer be uniform along the length of the roller (e.g., [8]); this can lead to edge buckling as shown, for example, by Lakshmikumaran and Wickert [9] or Banichuk *et al.* [10, 11]. Out-of-plane tilting of two adjacent rollers relative to each other induces a twisting deformation of the web surface, which presents yet another opportunity for wrinkling to develop [12, 13, 14].

Stability issues involving axially moving continua typically fall within the broad class of non-conservative problems (e.g., [15, 16, 17]). Although there is an extensive literature on band saw stability and vibrations (see the reviews [18, 19]), most of the early studies were carried out by using one-dimensional approximations (travelling strings and beams rather than plates). A notable exception is a paper by Ulsoy and Mote [20], in which the stability of a (non-uniformly) pre-stressed axially moving elastic strip was studied numerically by employing classical plate theory. In the same context, the case of uniform pre-stress was dealt with more extensively by Lin [21], who identified both the divergence and flutter critical speeds with the help of a similar numerical strategy.

For the past three decades there has been a significant growing interest in axially moving plate-like systems – a detailed assessment of this vast body of literature is beyond the scope of our present study. We refer to the recent comprehensive reviews [22, 23, 24, 25], which give a good picture of the status quo in this area. The recent books [10, 26] are also welcome additions to the literature, and should be consulted for more specialised accounts of past and present research.

In the current study we want to revisit the situation considered in [10] (and also in [11], pp. 345-364), in which the divergence buckling critical speeds of a non-uniformly tensioned web were found via a direct numerical approach. The scenario of interest involves a thin elastic plate subjected to linearly distributed tensile forces on two opposite edges, while the other two sides are traction-free. In the static case (i.e., zero axial speed) this particular configuration has previously been examined by Veits *et al.* [27] in relation to its natural frequency spectrum. Lin and Mote [28] also dealt with an apparently more general setting – in their work the aforementioned tensile loads were *nonlinearly* distributed along two opposite edges. However, this analysis was restricted to simply-supported boundary conditions on all edges, and the speed of the web was neglected. Our interest vis-à-vis the work reported in

[10] was originally kindled by the similarity between the equations discussed therein and a couple of our previous static wrinkling studies [29, 30]. Broadly speaking, one of the main ideas in what follows is to take advantage of the applied external tensile forces to show that, under suitably defined conditions, the corresponding new bifurcation problem can be reduced to a sequence of second-order "membrane"-type equations amenable to closed-form solutions. The upshot of this strategy is an analytical formula for the divergence buckling critical speeds which captures the dependence on the various parameters that define the configuration of interest here.

Given the context outlined above, we embark on our investigation in the next section by providing a brief summary of the main bifurcation problem. To motivate the specific types of deformations explored later in the paper, the qualitative behaviour of the numerical buckling modes is systematically illustrated in §3 by using some novel non-dimensional groups. The discussion of our asymptotic approximations of the numerical results is divided into two main distinct cases. The first asymptotic structure appears in §4 and deals with edge-localised deformations. As shown in §4.1, from a mathematical point of view, this consists of a hierarchy of second-order boundary-value problems which can be solved in terms of the usual Airy functions of the first kind (e.g., [31, 32]). These solutions need to be supplemented with additional information derived from a secondary bending boundary-layer located near one of the free edges of the plate; the relevant details appear in §4.2. A second regime, which corresponds largely to a weakly inhomogeneous axial tension, is also considered briefly in §5. It is shown therein that the critical eigenmodes have a structure that mirrors closely those of the uniformly tensioned plate (which was discussed in [33]). The paper concludes with a number of observations and some possible future extensions.

2 The key equations

To make this work reasonably self-contained, an overview of the mathematical model that will be the subject of our subsequent discussions is included below; further details can be found in [10, 11, 33].

The situation of interest is illustrated in Figure 1; it concerns an axially moving thin sheet stretched across two rollers. Let this rectangular sheet be modelled as a thin elastic plate of thickness $h > 0$ and width $2b > 0$, while the distance between the rollers is $\ell > 0$. Linear elasticity is assumed for the constitutive behaviour of the plate material, with E being its Young's modulus and ν the corresponding Poisson's ratio. A system of Cartesian axes (x, y, z) is then chosen so that x, y lie in the plane of the middle surface of the underformed plate, and z is in the direction normal to this plane – in this reference frame the mid-plane of the undeformed plate corresponds to the domain $0 \le x \le \ell$, $-b \le y \le b$. The plate is translated axially with a velocity $\boldsymbol{v}_0 = (V_0, 0, 0)$, where $V_0 > 0$.

The axial transport of the plate between the rollers is facilitated by the presence of a tension in the x-direction. It is usually assumed that the edges $x = 0$ and $x = \ell$ are subjected to in-plane forces consistent with such tension. The case of a *uniform* tension was considered in detail in [33] (see also [11]); here, on the other hand, we are interested in the scenario seen in Figure 1, in which the applied forces on the aforementioned edges are of the form $T_0 + \alpha y$, with $T_0, \alpha > 0$ given parameters. Letting $\mathring{N}_{xx}$, $\mathring{N}_{xy}$, $\mathring{N}_{yy}$ denote the in-plane (or membrane) forces in the stretched unbuckled plate, it can be trivially shown (e.g., [34]) that the pre-buckling stress distribution is given by

$$\mathring{N}_{xx} = T_0 + \alpha y\,, \qquad \mathring{N}_{xy} = \mathring{N}_{yy} = 0\,. \tag{2.1}$$

This spatially-dependent plane-stress solution represents the basic state for the bifurcation problem reviewed in the remaining of this section. It is noted that in order for the condition $\mathring{N}_{xx} > 0$ to be

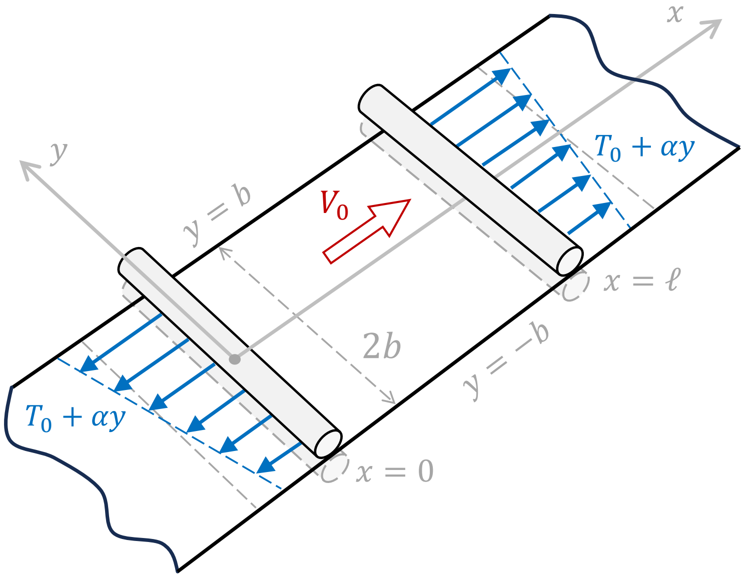

Figure 1: Non-uniformly tensioned thin elastic sheet in axial motion across two sets of rollers; the degree of non-uniformity is measured by the parameter $\alpha > 0$.

satisfied for all $|y| \leq b$, one needs

$$0 < \alpha < \alpha_{\max}\,, \qquad \text{with} \qquad \alpha_{\max} := T_0/b\,. \tag{2.2}$$

If the condition (2.2) is ignored then the buckling of the tensioned web may be directly related to the appearance of *static* compressive stresses due to the inhomogeneous pre-stressing. Indeed, this is the case studied by Lakshmikumaran and Wickert [9], who set $V_0 = 0$ right from the outset and treated α as the main eigenvalue of their bifurcation equation. It is perhaps worth emphasising that their work was apparently concerned with strips (i.e., the lengths of the plates considered were several times larger than their widths).

The previous stability analyses in [10, 11] were conducted upon the usual linearised Föppl-von Kármán equation (e.g., [38, 39, 40]) for the incremental out-of-plane displacement $w \equiv w(x, y)$,

$$\rho_M \frac{d^2 w}{dt^2} + D\nabla^4 w - \nabla_m^2 w = 0\,, \tag{2.3}$$

where $D \equiv Eh^3/12(1-\nu^2)$ represents the usual bending rigidity of the plate and ρ_M denotes the mass per unit area of its (undeformed) mid-surface. The acceleration term in this equation is calculated by using the so-called *(axially) co-moving derivative* operator (e.g., [11], pp. 235–237) indicated by d/dt; for a scalar field $\phi \equiv \phi(x, y, t)$ we mention the useful formula $d\phi/dt = (\boldsymbol{\nabla}\phi) \cdot \boldsymbol{v}_0 + \partial\phi/\partial t$, which can be used repeatedly to get an expanded version of the plate acceleration in terms of V_0. The other symbols in (2.3) correspond to various differential operators whose definitions are recorded below

$$\nabla^2 := \frac{\partial^2}{\partial x^2} + \frac{\partial^2}{\partial y^2}\,, \qquad \nabla^4 := \nabla^2\nabla^2\,, \qquad \nabla_m^2 := \mathring{N}_{xx}\frac{\partial^2}{\partial x^2} + 2\mathring{N}_{xy}\frac{\partial^2}{\partial x \partial y} + \mathring{N}_{yy}\frac{\partial^2}{\partial y^2}\,.$$

To complete the description of the bifurcation problem for the travelling web, suitable boundary conditions for the transverse displacement w must be specified. The plate edges that are in contact with the rollers ($x = 0$ and $x = \ell$, respectively) are taken to be simply supported, while the other two will be assumed traction-free. The equations for the latter correspond to the condition that the normal component of the bending moment and the effective shear must be zero on the free edges. Taken together, the above edge constraints translate into (e.g., [38])

$$w = \frac{\partial^2 w}{\partial x^2} = 0\,, \qquad x = 0,\, \ell \quad (-b \leq y \leq b)\,, \tag{2.4a}$$

$$\frac{\partial^2 w}{\partial y^2} + \nu \frac{\partial^2 w}{\partial x^2} = 0\,, \qquad y = \pm b \quad (0 \leq x \leq \ell)\,, \tag{2.4b}$$

$$\frac{\partial^3 w}{\partial y^3} + (2-\nu)\frac{\partial^3 w}{\partial x^2 \partial y} = 0\,, \qquad y = \pm b \quad (0 \leq x \leq \ell)\,. \tag{2.4c}$$

In the case of steady-state motion of a travelling web subjected to uniaxial tension in the x-direction, equation (2.3) reduces to

$$D\nabla^4 w - (\mathring{N}_{xx} - \rho_M V_0^2)\frac{\partial^2 w}{\partial x^2} = 0\,. \tag{2.5}$$

Comparison of (2.5) with other classical buckling equations in related scenarios (e.g., [5, 6]) indicates that the axial translation acts only to modify the effective tension in the plate. In this sense, identifying the critical speed at which the plate becomes unstable is entirely analogous to a study of the classical plate buckling problem.

Equations (2.3) and (2.4) can be cast in non-dimensional form by introducing the new quantities

$$\overline{x} := \frac{x}{\ell}\,, \qquad \overline{y} := \frac{y}{b}\,, \qquad \beta := \frac{\ell}{\pi b}\,, \tag{2.6a}$$

$$\lambda := \frac{\rho_M \ell^2}{\pi^2 D}\left(V_0^2 - \frac{T_0}{\rho_M}\right)\,, \quad \widetilde{\alpha} := \left(\frac{b\ell^2}{\pi^2 D}\right)\alpha\,, \quad \widetilde{\alpha}_{\max} := \frac{\ell^2 T_0}{\pi^2 D}\,. \tag{2.6b}$$

Note that the re-scaled independent variables will then satisfy $0 \leq \overline{x} \leq 1$ and $-1 \leq \overline{y} \leq 1$; to avoid complicating the notation unnecessarily, the 'bar' on x and y will be dropped henceforth. As already noted in reference [10], $\alpha/\alpha_{\max} = \widetilde{\alpha}/\widetilde{\alpha}_{\max}$, and the common value of these fractions is set to some $\eta \in [0, 1)$. In other words, $\widetilde{\alpha}$ is uniquely determined by specifying η and $\widetilde{\alpha}_{\max}$.

Owing to the simply-supported boundary condition (2.4a), solutions of the bifurcation equation will be sought in the form

$$w(x, y) = f(y)\sin(\pi x)\,, \tag{2.7}$$

for some function $f \equiv f(y)$ (yet to be found). Plugging (2.7) into (2.5), the governing equation for this unknown transverse amplitude becomes

$$\beta^4 \frac{d^4 f}{dy^4} - 2\beta^2 \frac{d^2 f}{dy^2} + (1 - \lambda + \widetilde{\alpha} y) f = 0\,, \qquad -1 < y < 1\,, \tag{2.8}$$

which is to be solved subject to the boundary conditions that follow from (2.4),

$$\beta^2 \frac{d^2 f}{dy^2} - \nu f = 0\,, \qquad y = \pm 1\,, \tag{2.9a}$$

$$\beta^2 \frac{d^3 f}{dy^3} - (2-\nu)\frac{df}{dy} = 0\,, \qquad y = \pm 1\,. \tag{2.9b}$$

For given ν, β, and $\widetilde{\alpha} \equiv \eta\,\widetilde{\alpha}_{\max}$, equations (2.8)-(2.9) define a boundary-value problem for the eigenparameter λ. It is perhaps worth re-iterating that the true eigenvalue in the present scenario is the speed $V_0 > 0$ rather than $\lambda \in \mathbb{R}$. Once we have identified the latter quantity, the critical speed is recovered by using the first definition in (2.6b). The parameter β can potentially take on a wide range of values, which are heavily influenced by the aspect ratio of the plate's middle-plane. For a strip one would expect $\beta \gg 1$, but our focus lies on a different class of structures known as *webs*; that is, we will consider configurations in which the width is greater than the length. Banichuk *et al.* [10, 11] used the numerical values $\ell = 0.1$ m, $b = 0.5$ m, which give $\beta \simeq 0.0637$. For the remaining of the current study ℓ and b will be assumed to be such that $\beta = \mathcal{O}(10^{-2})$ or even smaller. By making this choice we can regard β as a "small" parameter in equations (2.8)-(2.9). As we are going to see shortly, it is the singularly-perturbed nature of this eigenvalue problem that will make it possible to obtain useful approximations for the critical speed V_0. Before delving further into this matter, we take a brief detour to provide a general overview of the numerical solutions for the above boundary-value problem.

3 Numerical considerations

A limited number of numerical simulations of the bifurcation equation (2.8) subject to (2.9) were presented in reference [10] (and later reproduced in [11]). The specific numerical values considered were $T_0 = 500$ N/m, $\rho_M = 0.08$ Kg/m^2, $h = 10^{-4}$ m, $E = 10^9$ N/m^2, with ℓ and b as indicated at the end of the previous section. As for $\widetilde{\alpha}$, this was chosen to be a certain percentage of $\widetilde{\alpha}_{\max}$; more specifically, $\widetilde{\alpha} = \eta\,\widetilde{\alpha}_{\max}$ with $\eta \in \{0, 10^{-6}, 10^{-4}, 10^{-2}\}$. While the critical speeds V_0 in all these cases turned out to be very close to each other, the eigenmodal deformations displayed significant qualitative differences. For example, for $\eta = 10^{-6}$ the *critical* eigenmode (i.e., the one associated with the lowest positive V_0) consisted of an $\mathcal{O}(1)$ central part within the range $-1 \le y \le 1$, supplemented by two thin boundary layers near $y = \pm 1$. However, for $\eta = 10^{-4}$ the same eigenmode was localised near the edge $y = -1$, with negligibly small out-of-plane deformations occuring for $0 \le y \le 1$; such localisation phenomenon became progressively stronger as η increased to 10^{-2} (see Figures 6 and 7 in [10]). A rational explanation for this puzzling behaviour is missing from the references cited above; it is one of the goals of the present study to bridge this gap and offer plausible answers by utilising certain asymptotic arguments.

Motivated by past experience with related bifurcation problems (e.g., [29]) we introduce the reference parameter

$$\varepsilon^2 := \frac{\pi^2}{12(1-\nu^2)}\left(\frac{Eh}{T_0}\right)\left(\frac{h}{\ell}\right)^2, \tag{3.1}$$

which characterises the intensity of the background tension T_0 relative to the thinness of the web. For the parameter values mentioned above, simple calculations indicate that $\varepsilon^2 \simeq \mathcal{O}(10^{-4})$, so we will assume that $0 < \varepsilon \ll 1$. Of course, if $T_0 \to 0^+$ it is possible that $\varepsilon = \mathcal{O}(1)$ or it is even bigger, but this scenario would correspond to a slack web and does not fit the physics of the situation we are interested in. With this in mind, we claim that the two distinct types of behaviour mentioned above can be linked to the regimes identified below as (I) and (II),

$$(I)\ \frac{b\alpha}{T_0} = \mathcal{O}(\varepsilon^2)\,, \qquad (II)\ \frac{b\alpha}{T_0} = \mathcal{O}(\beta^2\varepsilon^2)\,. \tag{3.2}$$

Note that $b\alpha/T_0 = \alpha/\alpha_{\max} \equiv \eta$ represents a non-dimensional measure of the degree of inhomogeneity of the applied tension $T_0 + \alpha y$. Since β is small, the second situation above involves a weaker inhomogeneity than in the first scenario. The eigenmodes in Case (I) turn out to be localised near one of the free edges, but the situation is less straightforward for Case (II). For β moderately small one finds behaviour that is characteristic for $\alpha = 0$ (purely homogeneous tension) except for thin adjustment boundary-layers that become noticeable near both free edges. As β is reduced further the critical eigenmode becomes again localised near the edge $y = -1$. These behaviours will be illustrated below for easy reference.

Letting $C_0 := \sqrt{T_0/\rho_M}$, the speed V_0 in (2.6b) can be expressed as

$$V_0 = C_0\sqrt{1 + \lambda\varepsilon^2}\,; \tag{3.3}$$

this simple formula explains why the critical speeds found in [10] were very similar to those associated with the homogeneous case ($\alpha = 0$). Even though the eigenvalues determined from the solution of (2.8)-(2.9) might be vastly different for various values $0 < \eta < 1$, their contribution to the critical speed will be offset by the ε^2-term that appears under the square root in (3.3). Regarding the approach to approximating λ using an asymptotic series, this implies that there is no need to compute more than one or two terms to achieve a reasonably precise estimate for the critical speed. However, from a mathematical standpoint, it remains desirable to gain a deeper comprehension of the fundamental asymptotic framework underlying the perturbed eigenvalues λ and their associated eigenmodes.

To better appreciate the features of the bifurcation problem summarised in the previous section, we will first review quickly some of the key properties of the numerical solutions for the *homogeneous case* (covered in [11, 33]). In this scenario $\alpha = 0$ in (2.1), and the resulting situation is fairly standard since the differential equation (2.8) allows for an elementary solution in closed-form. As explained in [10], the homogeneous version of (2.8)-(2.9) admits two monotonically increasing sequences of eigenvalues (and distinct eigenmodes), which can be classified as either *symmetric* or *anti-symmetric* (with respect to $y = 0$); we will denote these by $\lambda_s^{(k)}$ and $\lambda_a^{(k)}$ ($k = 1, 2, \dots$), respectively. It was noticed in the aforementioned reference that

$$0 < \lambda_s^{(1)} < \lambda_a^{(1)} < 1 \qquad \text{and} \qquad \lambda_s^{(1)}, \lambda_a^{(1)} \to \lambda_* < 1 \quad \text{as} \quad \beta \to 0^+\,, \tag{3.4}$$

where the expression of λ_* depends on the Poisson's ratio only, and its precise expression will be given shortly. The spectrum of the bifurcation problem contains also infinitely many elements in $(1, +\infty)$, but those values are less important in problems of elastic stability as one is mostly concerned with the lowest point of the discrete spectrum. We include in Figure 2 examples of eigenmodes for the first and second smallest symmetric eigenvalues when $\nu = 0.3$. As $\beta \to 0^+$, the modes associated with $\lambda_s^{(1)}$ become progressively flatter over most of the range $-1 < y < +1$ except near $y = \pm 1$, where sharp boundary-layers exist. By contrast, the eigenmodes related to $\lambda_s^{(2)}$ consist of an $\mathcal{O}(1)$ core-type structure, also augmented by thin boundary layers near the free edges of the plate. A few samples of anti-symmetric modes for $\lambda_a^{(1)}$ and $\lambda_a^{(2)}$ are included in Figure 3. The numerical values of the eigenvalues associated with the modes shown in the last two Figures are recorded in Table 1. Additional results not included here confirm that $\lambda_s^{(2)}$, $\lambda_a^{(2)} \to 1^+$ as $\beta \to 0^+$.

The asymptotic limit of the critical eigenvalue $\lambda_* := \lim_{\beta\to 0^+} \lambda$ – mentioned in (3.4), can be obtained by a very simple boundary-layer argument. Introducing $\zeta \equiv \beta^{-1}(1+y) = \mathcal{O}(1)$ $(0 < \beta \ll 1)$, we note that under the assumption $\lambda < 1$, the transformed version of equation (2.8) with $\alpha = 0$ will admit a solution of the form

$$f(\zeta) = C_1 \exp(-\zeta\sqrt{1-\gamma}) + C_2 \exp(-\zeta\sqrt{1+\gamma})\,, \qquad (0 < \lambda =: \gamma^2;\, C_1,\, C_2 \in \mathbb{R})\,.$$

Table 1: Numerical eigenvalues for the homogeneous case of (2.8)-(2.9) when $\nu = 0.3$.

β	$\lambda_s^{(1)}$	$\lambda_s^{(2)}$	$\lambda_a^{(1)}$	$\lambda_a^{(2)}$
0.03	0.995522202	1.012346719	0.997298920	1.034471359
0.02	0.996032234	1.004577722	0.996417302	1.014257837
0.01	0.996205824	1.000796431	0.996210699	1.002976868

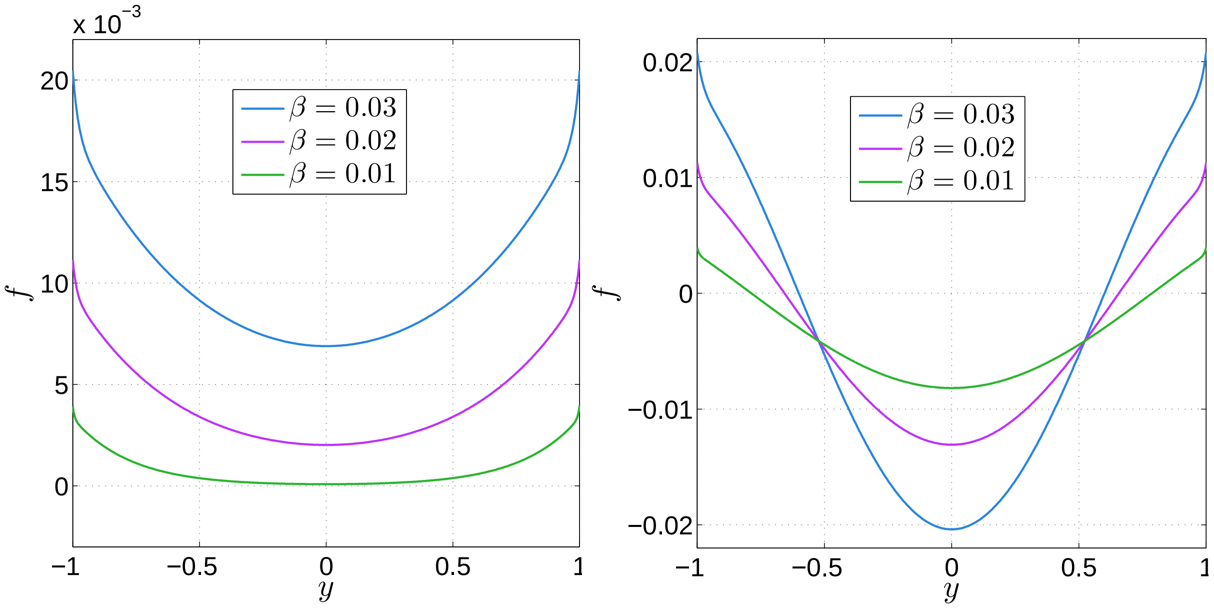

Figure 2: Examples of the first two *symmetric* modes of (2.8)-(2.9) in the case of homogeneous tension (i.e., $\alpha = 0$) and $\nu = 0.3$. The functions on the left correspond to $\lambda_s^{(1)}$, while those on the right are associated with $\lambda_s^{(2)}$.

Further use of the boundary conditions (2.9) results in a system two algebraic equations for the constants C_j $(j = 1, 2)$ that appear in the above expression,

$$C_1\sqrt{1-\gamma}\,(1-\nu+\gamma) + C_2\sqrt{1+\gamma}\,(1-\nu-\gamma) = 0\,, \tag{3.5a}$$

$$C_1(1-\nu-\gamma) + C_2(1-\nu+\gamma) = 0\,. \tag{3.5b}$$

The determinant of the coefficient matrix of this homogeneous linear system must vanish, thus leading to a simple equation in γ^2; the solution of interest, γ_* (say), eventually yields the desired asymptotic value of the lowest λ as $\beta \to 0^+$ via the relationship $\lambda = \lambda_* \equiv \gamma_*^2$, where

$$\lambda_* \equiv (1-\nu)\big(3\nu - 1 + 2\sqrt{1-2\nu+2\nu^2}\big)\,. \tag{3.6}$$

In obtaining λ_* we have considered the boundary-layer near $y = -1$; an identical result follows by repeating the above argument for the other boundary-layer near $y = 1$. For $\nu = 0.3$ formula (3.6) gives $\lambda_* \simeq 0.99620823$, which should be compared to the values listed in the first and third columns

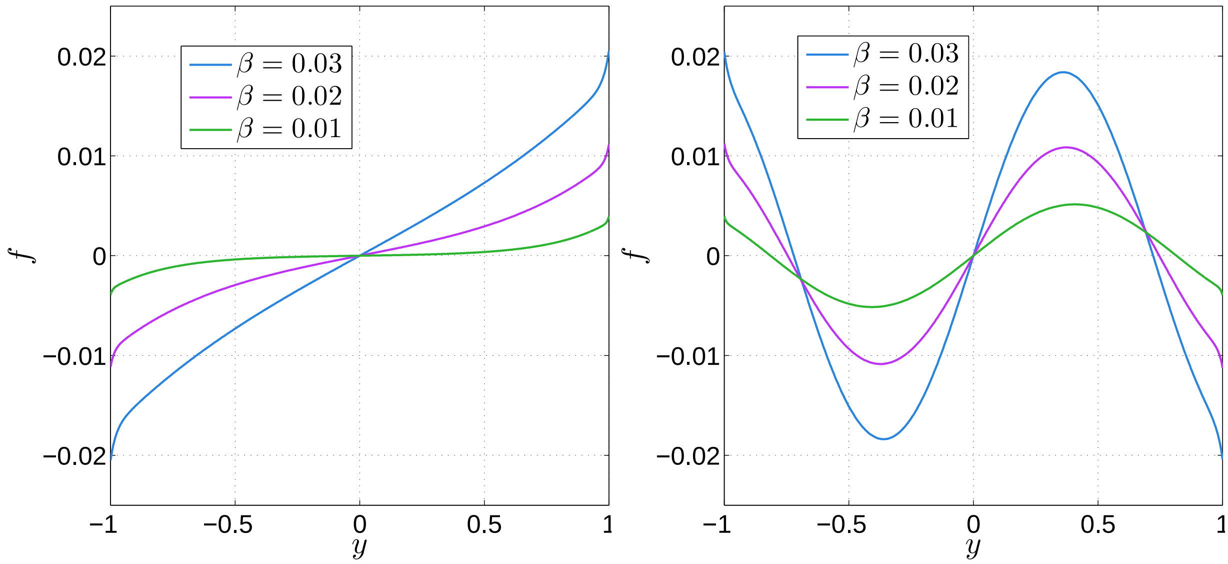

Figure 3: Same as per Fig. 2, except that here we show the *anti-symmetric* modes associated with $\lambda_a^{(1)}$ (left) and $\lambda_a^{(2)}$ (right).

of Table 1; further numerical work indicates that $\lambda_s^{(1)} \to \lambda_*^-$ and $\lambda_a^{(1)} \to \lambda_*^+$ as $\beta \to 0^+$. A close inspection of the exact determinantal equation used in reference [33] confirms that if the eigenvalues $\lambda_j^{(1)}$ $(j \in \{s, a\})$ of the homogeneous tension problem are regarded as functions of $0 < \beta \ll 1$, then their asymptotic behaviour is of the form $\lambda_j^{(1)} = \lambda_* \pm \ldots$, where the dots stand for transcendentally small terms.

A first set of samples of eigenmodes associated with the smallest and second smallest eigenvalues of the bifurcation problem (2.8)-(2.9) for *Case (II)* is included in Figure 4. In the interest of brevity, the Poisson's ratio has been set to a fixed value ($\nu = 0.3$); the results shown therein are representative for other standard values of this parameter provided that $\nu \neq 0$. We have chosen a typical (small) value for ε^2 and selected $\eta \equiv \widetilde{\alpha}/\widetilde{\alpha}_{\max}$ consistent with the second scenario proposed in (3.2). Taken at face value, the situation in *Case (II)* represents a weak perturbation of the homogeneous-tension problem reviewed in Figs. 2 and 3. For "moderately" small β's, the deformation in both windows appears to spread out across the entire lateral span of the web; also, the regions near the lateral edges of the plate are indicative of some sort of boundary-layers. Figure 5 depicts what happens to the dispersed modes recorded in the preceding Figure as β is reduced even more. The numerical data provides compelling evidence that the critical eigenmodes gradually become highly localized near the edge $y = -1$. Regarding the second mode (right window, same Figure), it predominantly exhibits a flat pattern, with localized deformations now present near the edge $y = 1$. Table 2 includes the eigenvalues of the modes seen in Figs. 4 and 5 – these are indicated by $\lambda^{(j)}$ $(j = 1, 2)$; for the sake of completeness, the next two eigenvalues ($\lambda^{(3)}$ and $\lambda^{(4)}$) are recorded as well. The eigenfunctions for these eigenvalues are not shown here since they are very similar to the second symmetric and anti-symmetric modes in the case $\alpha = 0$ (see the right windows of Figs. 2 and 3, respectively).

Although *Case (I)* can still be viewed as a perturbation of the uniform-tension scenario, this perturbation is no longer weak. In fact, the presence of the variable term $\widetilde{\alpha}y$ now completely alters the structure of the discrete spectrum for the eigenproblem (2.8)-(2.9) with $\alpha = 0$. To emphasize this argument, in Figure 6 we present instances of the eigenmodes associated with the smallest first three eigenvalues in *Case (I)*. The curves seen there confirm the edge-localised nature of the critical

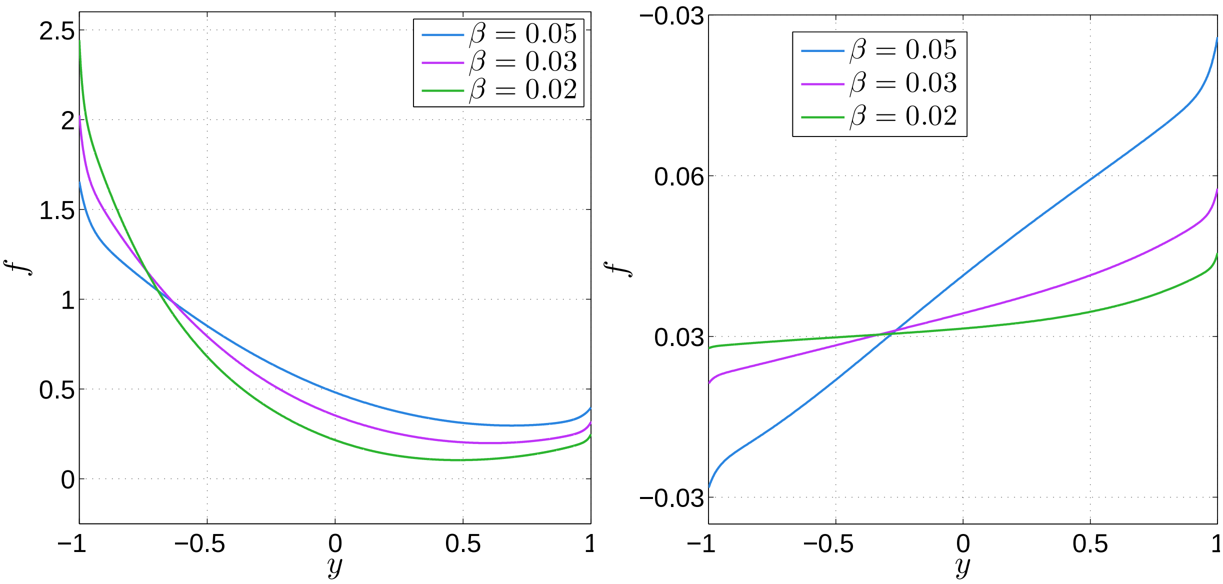

Figure 4: Eigenmodes of the bifurcation problem (2.8)-(2.9) for $\varepsilon^2 = 5 \times 10^{-5}$ and $\nu = 0.3$; all these eigenfunctions correspond to the smallest first two eigenvalues with $\lambda < 1$ in *Case (II)*. Examples of the *critical mode* appear in the left window and are obtained for $\eta = 3\beta^2\varepsilon^2 \simeq \mathcal{O}(\beta^2\varepsilon^2)$, with the chosen values of β recorded in the legend. The right window contains the corresponding modes for the second smallest eigenvalue with $\lambda < 1$.

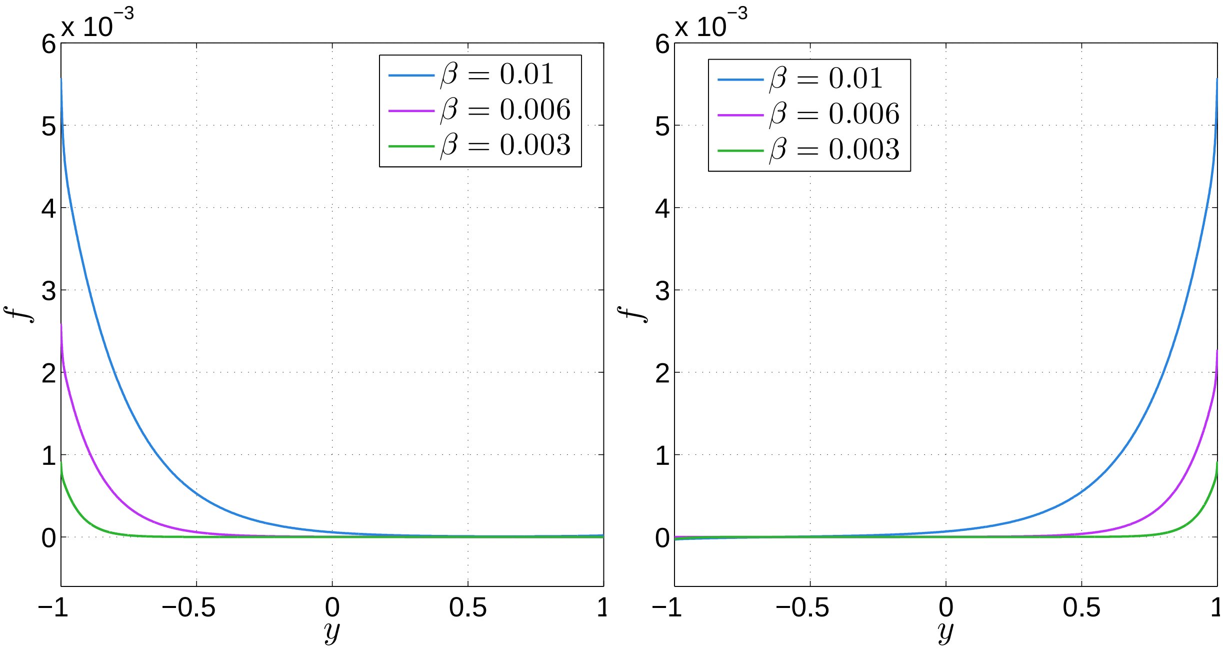

Figure 5: Examples of asymptotic shapes (as $\beta \to 0^+$) for the eigenmodes recorded in Figure 4.

eigen-deformations; a phenomenon that becomes progressively more pronounced as β gets smaller. Notwithstanding the apparent similarity between the edge-localisation seen in both cases, the asymptotic structure of the corresponding eigenmodes is essentially quite different as we are going to see shortly.

Table 2: Numerical eigenvalues for *Case (II)* when $\eta = 3\beta^2\varepsilon^2 \simeq \mathcal{O}(\beta^2\varepsilon^2)$ and $\nu = 0.3$; $\lambda^{(j)}$ $(j = 1, 2, 3, 4)$ represent the first four consecutive points in the discrete spectrum of the eigenproblem (2.8)-(2.9).

β	$\lambda^{(1)}$	$\lambda^{(2)}$	$\lambda^{(3)}$	$\lambda^{(4)}$
0.05	0.991618867	1.003907307	1.039820458	1.102040158
0.03	0.994267417	0.998491465	1.012358794	1.034484086
0.02	0.995260774	0.997175205	1.004571487	1.014261794
0.01	0.995941831	0.996474357	1.000792504	1.002977529
0.006	0.996107555	0.996308940	1.000234906	1.000931704
0.003	0.996182154	0.996234324	1.000050571	1.000204215

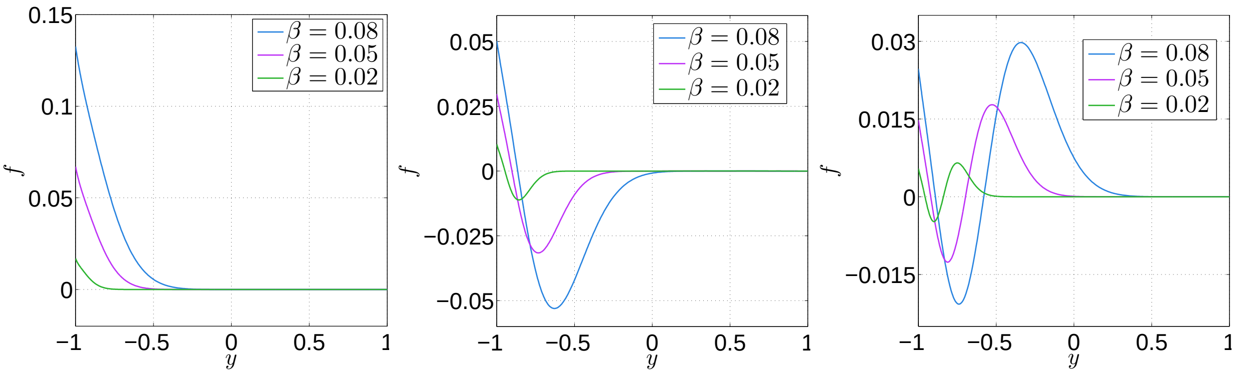

Figure 6: Samples of the first three eigenmode related to *Case (I)* for $\nu = 0.3$, and $\eta = 3\varepsilon^2 \simeq \mathcal{O}(\varepsilon^2)$; the critical modes appear in the leftmost window. The degree of localisation experienced by all three sets of curves becomes stronger as β decreases.

The numerical results included in this section have confirmed the overall features of the eigenmodes for the two proposed regimes (3.2). With this in mind, we are now ready to take a closer look at the corresponding asymptotic structures underlying each case.

4 The asymptotic structure for Case (I)

In this scenario the eigendeformation of the plate consists of two nested boundary layers of sizes $\mathcal{O}(\beta^p)$, with $p = 2/3$ and $p = 1$, respectively. For the sake of clarity, the corresponding mathematical details for these two asymptotic structures will be considered separately next.

4.1 The main layer

To identify the thickness of the boundary-layer in this case, we assume $0 < \beta \ll 1$ and introduce the new independent variable $0 < Y = \mathcal{O}(1)$ defined by $y = -1 + \beta^q Y$, where $q > 0$ is to be identified as explained below. The three terms on the left-hand side of equation (2.8) will be denoted by T_j $(j = 0, 2, 4)$ – according to the order of the derivatives present in each of them. The sizes of these terms are readily found to be $T_4 = \mathcal{O}(\beta^{4-4q})$, $T_2 = \mathcal{O}(\beta^{2-2q})$, and $T_0 = \mathcal{O}(1) + \mathcal{O}(\beta^q)$. Possible *distinguished limits* (i.e., acceptable values of $q > 0$) are found by a simple dominant-balance argument. Clearly, the balancing with the $\mathcal{O}(1)$-part of T_0 of either T_2 or T_4 yields only $q = 1$. Thus, $T_4 \sim T_2 = \mathcal{O}(1)$ and the constant part of T_0 is also $\mathcal{O}(1)$. Writing $\lambda = \lambda_0 + \dots$, where the 'dots' stand for higher-order terms, results in a re-scaled leading-order differential equation with constant coefficients of the same type as in the homogeneous case (i.e., $\alpha = 0$), subject to the change $\lambda \to \widetilde{\lambda} \equiv \lambda_0 + \widetilde{\alpha}$. Unlike the discussion in the previous section, one has to allow for $\widetilde{\lambda} > 1$ as well. Trivial calculations show that there are no solutions which experience exponential decay as $Y \to +\infty$ (see Figure 6) and which can also satisfy the transformed version of the constraints (2.9) at $Y = 0$. The conclusion that transpires from this brief discussion is that the simultaneous balancing of the above three terms is not a feasible option in Case (I). If $T_4 = \mathcal{O}(\beta^q)$ we find $q = 4/5$, but this value leads to $T_2 \gg T_j$ $(j = 0, 4)$, so it can be safely discarded. If $T_2 = \mathcal{O}(\beta^q)$ then $q = 2/3$; such a choice will result in an approximation for the original bifurcation equation that exhibits the required spatial variation in the T_0 term. It is perhaps worth emphasising that with this choice the largest term in the re-scaled (2.8) is the $\mathcal{O}(1)$-part of T_0, which has to vanish first. We can thus write

$$y = -1 + \beta^{2/3} Y \,, \qquad \text{with} \qquad Y = \mathcal{O}(1) \,. \tag{4.1}$$

The only other option left is $T_4 \sim T_2$, whereby $q = 1$; note that T_0 does not contribute to the leading-order approximation in this situation. The corresponding reduced equation is of fourth-order, and represents an inner-type approximation that will be taken up in §4.2.

Returning to the choice identified in (4.1), solutions of the bifurcation problem will be sought with an ansatz of the form

$$f = F_0(Y) + \beta^{\,1/3} F_1(Y) + \beta^{\,2/3} F_2(Y) + \dots \,, \tag{4.2a}$$

$$\lambda = \lambda_0 + \lambda_1 \, \beta^{\,2/3} + \lambda_2 \, \beta + \dots \,, \tag{4.2b}$$

in which the functions $F_j \equiv F_j(Y)$ and the coefficients λ_j $(j = 0, 1, 2, \dots)$ are to be found by substituting (4.2) in (2.8). At leading order this process results in an algebraic relation that is subsequently followed by a series of variable-coefficient differential equations

$$\big(1 - \widetilde{\alpha} - \lambda_0\big) F_0 = 0 \,, \tag{4.3a}$$

$$\mathcal{L}_{\rm out}[F_0] = \frac{1}{2}(1 - \widetilde{\alpha} - \lambda_0) F_2 \,, \tag{4.3b}$$

$$\mathcal{L}_{\rm out}[F_{j-1}] = \mathcal{R}_j \,, \qquad (j = 2, 3, \dots) \,, \tag{4.3c}$$

where

$$\mathcal{L}_{\rm out} \equiv \frac{d^2}{dY^2} - \frac{1}{2}\big(\widetilde{\alpha}\, Y - \lambda_1\big) \tag{4.4}$$

and

$$\mathcal{R}_2 \equiv -\frac{1}{2}\lambda_2 F_0 \,, \qquad \mathcal{R}_3 \equiv -\frac{1}{2}\lambda_3 F_0 - \frac{1}{2}\lambda_2 F_1 + \frac{1}{2}\left(\frac{d^4 F_0}{dY^4}\right) , \dots \,. \tag{4.5}$$

The solution of (4.3a) is simply

$$\lambda_0 = 1 - \widetilde{\alpha} \,, \tag{4.6}$$

and we note that (4.3b) then becomes a homogeneous second-order differential equation; furthermore, in writing out the expressions (4.5) this observation has also been taken into account.

On defining $\omega := (\widetilde{\alpha}/2)^{1/3}$ and introducing the change of variable

$$Z := \omega Y - \frac{\lambda_1}{2\omega^2} \,, \tag{4.7}$$

it follows immediately from (4.3b) that $\widehat{F}_0(Z) \equiv F_0(Y(Z)) = \mathrm{Ai}(Z)$, where 'Ai' denotes the usual Airy function that decays exponentially quickly as $Z \to +\infty$. The (arbitrary) constant of proportionality in this solution has been chosen to be unity. It is clear that this function cannot satisfy both boundary conditions (2.9) at $Y = 0$, but we note that the dominant contribution in those equations comes from the term $(2-\nu)(df/dy)$. Thus, we require $d\widehat{F}_0/dZ = 0$ at $Y = 0$, whereby

$$\lambda_1 = 2\zeta_{01}\omega^2 \,, \tag{4.8}$$

with $(-\zeta_{01}) \simeq (-1.0188)$ being the first zero of the *derivative* of the Airy function of the first kind, i.e. $\mathrm{Ai}^{(1)}(-\zeta_{01}) = 0$. Here (and in what follows) the superscripts on a function of Z indicate differentiation with respect to this variable. The determination of λ_j $(j = 2, 3, \dots)$ in the proposed approximation for the eigenparameter – see (4.2b), can be carried out systematically by solving the higher-order equations in (4.3c) subject to asymptotic matching with the solution developed later in §4.2.

The governing equation for $F_1(Y)$ is obtained by taking $j = 2$ in (4.3c). With the help of the transformation (4.7) this can be cast as a standard inhomogeneous Airy equation; a particular solution $\widehat{F}_1(Z) \equiv F_1(Y(Z))$ consistent with the localised behaviour we are interested in is given by

$$\widehat{F}_1(Z) = a_1 \mathrm{Ai}^{(1)}(Z) \,, \qquad \text{with} \quad a_1 := -\frac{\lambda_2}{2\omega^2} \,. \tag{4.9}$$

Note that this solution satisfies

$$\widehat{F}_1\Big|_{Z=-\zeta_{01}} = 0 \qquad \text{and} \qquad \frac{d\widehat{F}_1}{dZ}\Big|_{Z=-\zeta_{01}} = \left(\frac{\lambda_2\zeta_{01}}{2\omega^2}\right)\mathrm{Ai}_0 \,, \tag{4.10}$$

where $\mathrm{Ai}_0 \equiv \mathrm{Ai}(-\zeta_{01})$.

The function $F_2(Y)$ in (4.2a) is similarly identified by considering the equation (4.3c) for $j = 3$. Following the same strategy as above, it can be shown that a particular solution $\widehat{F}_2(Z) \equiv F_2(Y(Z))$ is

$$\widehat{F}_2(Z) = a_2 Z \mathrm{Ai}(Z) + \left(a_3 + a_4 Z^2\right)\mathrm{Ai}^{(1)}(Z) \,, \tag{4.11}$$

where

$$a_2 := \frac{2\omega^2}{5} + \frac{\lambda_2^2}{8\omega^4} \,, \qquad a_3 := -\frac{\lambda_3}{2\omega^2} \,, \qquad a_4 := \frac{\omega^2}{10} \,.$$

For future reference we also remark that

$$\widehat{F}_2\Big|_{Z=-\zeta_{01}} = -\zeta_{01}\left(\frac{2\omega^2}{5} + \frac{\lambda_2^2}{8\omega^4}\right)\mathrm{Ai}_0 \,. \tag{4.12}$$

The process illustrated above can be continued indefinitely. Note that the original boundary condition (2.9) at $y = -1$ had to be discarded for F_1 and F_2, an observation that suggests the need to explore a secondary asymptotic structure adjacent to the edge $y = -1$ of the rescaled plate. This point will be taken up and dealt with next.

4.2 The secondary layer

In the given context (the small-β regime), strong bending effects are primarily localized within a narrow boundary layer, which has a characteristic size of approximately $\mathcal{O}(\beta)$. This thin (inner) zone is attached to one of the plate's free edges and extends across the two rollers seen in Figure 1. With this in mind, we begin by introducing the re-scaled variable $\overline{Y} > 0$ such that

$$y = -1 + \beta\,\overline{Y} \,, \qquad \text{with} \qquad \overline{Y} = \mathcal{O}(1) \,. \tag{4.13}$$

The inner-layer solution will be sought with an ansatz of the form

$$f = f_{\mathrm{inn}} \equiv f_0(\overline{Y}) + \beta^{2/3} f_1(\overline{Y}) + \beta f_2(\overline{Y}) + \dots\,, \tag{4.14}$$

in which the functions f_j $(j = 0, 1, 2, \dots)$ will be determined sequentially by solving a hierarchy of fourth-order differential problems; as $\overline{Y} \to +\infty$, it is also necessary for these solutions not to exhibit exponential growth.

The usual substitutions lead to the following sequence of equations

$$\mathcal{L}_{\mathrm{inn}}[f_j] = \widetilde{\mathcal{R}}_j\,, \qquad \mathcal{L}_{\mathrm{inn}} \equiv \frac{d^4}{d\overline{Y}^4} - 2\frac{d^2}{d\overline{Y}^2}\,, \qquad (j = 0, 1, 2, \dots)\,, \tag{4.15}$$

in which the first two right-hand sides $\widetilde{\mathcal{R}}_j$ assume the following expressions

$$\widetilde{\mathcal{R}}_0 \equiv 0\,, \qquad \widetilde{\mathcal{R}}_1 \equiv \lambda_1 f_0\,, \dots\,. \tag{4.16}$$

The equations (4.15) must be solved subject to the constraints (2.9) applied at $\overline{Y} = 0$. In addition, to fully specify the functions f_j, the elementary solution of the above boundary-value problems is not enough – we must also take advantage of the information derived in the previous section in order to asymptotically match the appropriate contributions from both boundary-layers. Defining f_{out} as the solution f in the ansatz (4.2a), and noting that $Y = \beta^{1/3}\,\overline{Y}$, we have

$$f_{\mathrm{out}} = \Pi_{00} + \underline{\left(\Pi_{10} + \omega \Pi_{01} \overline{Y}\right)} \beta^{1/3} + \left(\Pi_{20} + \omega \Pi_{11} \overline{Y} + \frac{1}{2}\omega^2 \Pi_{02} \overline{Y}^2\right) \beta^{2/3} + \dots\,, \tag{4.17}$$

where the constants $\Pi_{kj} \in \mathbb{R}$ are defined by

$$\Pi_{kj} := \begin{cases} \left.\dfrac{d^j \widehat{F}_k}{dZ^j}\right|_{Z=-\zeta_{01}} & \text{if} \quad j \geq 1\,, \\ \widehat{F}_k(-\zeta_{01}) & \text{if} \quad j = 0\,. \end{cases}$$

We remark in passing that all the Π-coefficients written down in (4.17) can be calculated with the help of the expressions (4.9) and (4.11) from §4.1. In particular, the underlined $\mathcal{O}(\beta^{1/3})$-part of (4.17) will drop out since $\Pi_{10} = \Pi_{01} = 0$.

The leading-order term in (4.14) is routinely found by solving (4.15) with $j = 0$. Leaving out the exponentially growing part of the obtained solution, the final result is

$$f_0(\overline{Y}) = c_1 \exp\left(-\overline{Y}\sqrt{2}\right) + c_2 + c_3 \overline{Y}\,, \tag{4.18}$$

where $c_j \in \mathbb{R}$ $(j = 1, 2, 3)$. We recall that the leading-order term in the outer solution (i.e., F_0) was forced to satisfy (2.9b), so the leading-order contribution to the inner solution must comply with the other boundary condition (2.9a). This gives a linear relationship between c_1 and c_2, but c_3 remains arbitrary. Matching (4.17) and (4.18) requires $c_3 = 0$, while the remaining two constants can be shown to be

$$c_1 = \frac{\nu \mathrm{Ai}_0}{2 - \nu} \qquad \text{and} \qquad c_2 = \mathrm{Ai}_0\,. \tag{4.19}$$

To find f_1 we must solve (4.15) with $j = 1$; this will require the expression (4.18). The general solution of this equation can be shown to be

$$f_1(\overline{Y}) = (c_4 \overline{Y} + c_5) \exp\left(-\overline{Y}\sqrt{2}\right) - \frac{1}{4}\underline{\lambda_1 \mathrm{Ai}_0 \overline{Y}^2} + c_6 + c_7 \overline{Y}\,, \tag{4.20}$$

where

$$c_4 := -\frac{\nu\lambda_1 \mathrm{Ai}_0}{4\sqrt{2}(2-\nu)}\,, \qquad c_5 := \frac{c_8}{2} - \frac{5\nu\lambda_1\mathrm{Ai}_0}{16(2-\nu)}\,,$$

and the constants c_6, c_7, $c_8 \in \mathbb{R}$ are determined as explained next. Applying the boundary conditions (2.9) gives

$$c_8 := \frac{2\nu c_6}{2-\nu} + \frac{\lambda_1(16-6\nu-5\nu^2)\mathrm{Ai}_0}{8(2-\nu)^2}\,, \qquad c_7 := -\frac{\nu^2\sqrt{2}c_6}{(2-\nu)^2} + \frac{\lambda_1\nu(\nu^2+10\nu-16)\mathrm{Ai}_0}{4\sqrt{2}(2-\nu)^3}\,. \tag{4.21}$$

The first of these two constants (c_8) is inconsequential for our immediate purposes, but we remark that c_7 will have to match the linear part of the $\mathcal{O}(\beta^{2/3})$-term in the asymptotic result (4.17). An important observation at this juncture is that the quadratic term in that expansion is identical to the (underlined) one in (4.20), a fact that reinforces the consistency of our asymptotic expansions. Further noting that $c_6 = \Pi_{20}$, use of (4.10) and (4.12) in conjunction with the matching requirement mentioned above leads to a quadratic equation in λ_2,

$$\mathcal{H}_{22}\lambda_2^2 + \mathcal{H}_{21}\lambda_2 + \mathcal{H}_{20} = 0 \tag{4.22}$$

in which

$$\mathcal{H}_{22} := 5\nu^2(2-\nu)\,, \qquad \mathcal{H}_{21} := -10\sqrt{2}(2-\nu)^3\omega^3\,, \qquad \mathcal{H}_{20} := -2\nu(3\nu^2-66\nu+80)\omega^6\,.$$

The solution of interest (i.e., the smallest in absolute value) can be cast in the form

$$\lambda_2 = \frac{\omega^3}{\nu^2}\left[\sqrt{2}(2-\nu)^2 - \frac{2\sqrt{\mathcal{Q}(\nu)}}{\sqrt{5(2-\nu)}}\right]\,, \tag{4.23}$$

with $\mathcal{Q}(s) \equiv 80 - 200s(1-s) - 60s^3 - 8s^4 - s^5$ a polynomial in $s \in \mathbb{R}$. For $0 \le s \le (1/2)$ it is easily checked that $Q(s) > 0$, i.e. the expression in (4.23) is real-valued.

The discussion of *Case (I)* will now be completed with a brief illustration of the accuracy of the formulae obtained thus far. To this end, we include in Figure 7 comparisons between the predictions provided by the two- or three-term result (4.2b) and the eigenvalues of the main bifurcation problem as follow from full numerical simulations; there are two types of comparisons included therein. In the left window we have chosen $\beta = 0.05$ and $\nu = 0.3$, but the agreement between the three sets of data is representative for other values $0.01 \le \beta \le 0.09$. It is clear that both types of approximations perform quite well, although the three-term predictions are better since they lead to relative accuracy less than 1%. The results included in the window on the right correspond to fixing $\eta = 4.1\varepsilon^2$ (with $\varepsilon^2 \simeq 5\times10^{-5}$) and varying β as indicated on the horizontal axis. The relative accuracy of the comparisons seen there ranges between 0.75% and 0.42%. As a side note, it is worth mentioning that both curves gradually converge in tandem towards the value $\lambda_0 = -3.1$ as $\beta^{-1} \to +\infty$.

Two final caveats pertain to the preceding work. Initially, we established at the beginning of §4.1 that β would be treated as a small parameter. A cursory examination of the expansion (4.2b) implies that, formally, the applicability of the discussed asymptotic analysis requires the stronger condition $0 < \beta^{1/3} \ll 1$. In light of this observation we are fortunate that the agreement between the numerics and asymptotics is as good as seen in Figure 7. The second observation we want to make is about the asymptotic character of the aforementioned ansatz. According to (4.6), the first two terms in that series become comparable when $\widetilde{\alpha} \simeq 1$ or, more precisely, if $1 - \widetilde{\alpha} \simeq \mathcal{O}(\beta^{2/3})$. This aspect will not be pursued here because this is a very unlikely scenario, and our additional numerical simulations

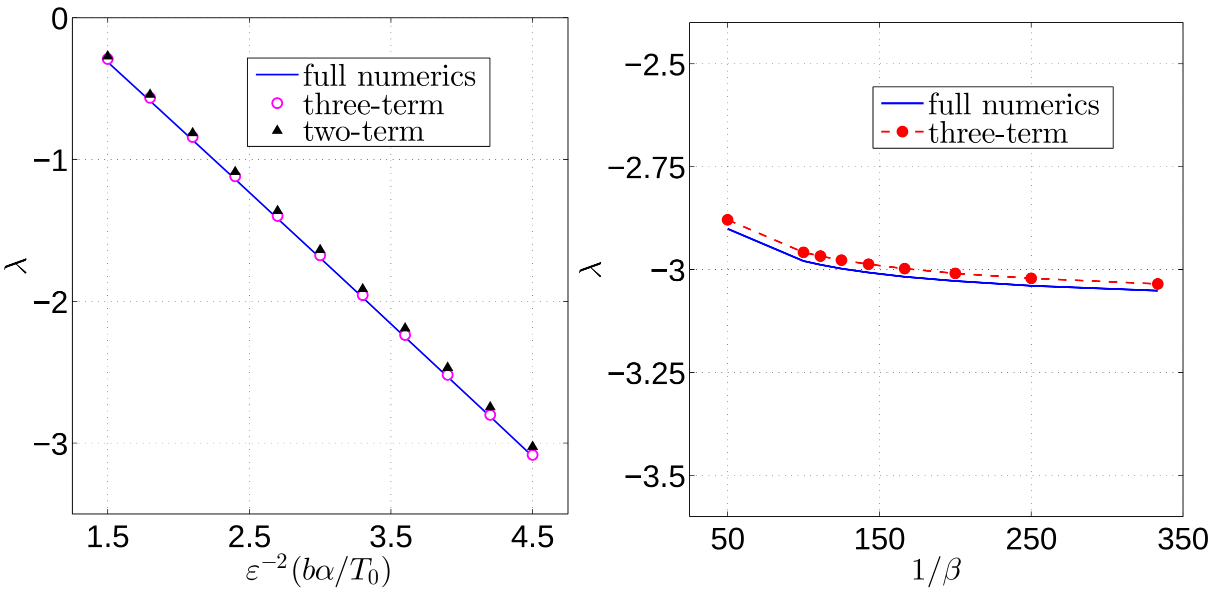

Figure 7: Examples of comparisons between the asymptotic formulae for *Case (I)* and the eigenvalues of boundary-value problem (2.8)-(2.9) obtained by direct numerical simulations. The results on the left correspond to $\beta = 0.05$ and include both the two- and three-terms asymptotic approximations (shown as markers). On the right, $b\alpha/T_0 = 4.1\varepsilon^2 \simeq \mathcal{O}(\varepsilon^2)$ and we vary $\beta = 0.02, 0.01, 0.009, \ldots, 0.003$. In both windows $\nu = 0.3$.

have indicated no significant qualitative differences in the shape of the eigenmodes. However, it is of interest to note that the agreement in the left window of Figure 7 improves as $\widetilde{\alpha} \equiv \varepsilon^{-2}(b\alpha/T_0)$ moves further away from unity. This is related to the presence of a *turning* (or *transition*) point in the differential equation (2.8). Letting y_0 denote this quantity, use of (4.2b) in conjunction with (4.6) and (4.8) gives

$$y_0 \equiv -(1-\lambda)/\widetilde{\alpha} = -1 + \left(\zeta_{01}\sqrt[3]{2/\widetilde{\alpha}}\right)\beta^{2/3} + \ldots\,;$$

thus, for a fixed β, $y_0 \to -1^+$ as $\widetilde{\alpha} \to +\infty$. In other words, the turning point will shift towards the edge $y = -1$ as $\widetilde{\alpha}$ gets larger, which in turn will enhance the degree of localisation that the web undergoes near that specific position.

5 The asymptotic structure for Case (II)

In §4 we have worked under the assumption that $\eta = \mathcal{O}(\varepsilon^2)$, so $\widetilde{\alpha} \equiv \eta\,\widetilde{\alpha}_{\max} = \mathcal{O}(1)$. For the situation investigated below, according to (3.2), we need to consider $\eta = \mathcal{O}(\beta^2\varepsilon^2)$ and therefore $\widetilde{\alpha} = \mathcal{O}(\beta^2)$; this suggests writing $\widetilde{\alpha} = \alpha_0\beta^2$, for some $\alpha_0 = \mathcal{O}(1)$.

The numerical evidence presented in §3 has revealed that when $\alpha = 0$ the main eigenproblem (2.8)-(2.9) admits a discrete spectrum consisting of two eigenvalues located in the interval $(0,1)$; it has been also pointed out that there is an additional infinite sequence of eigenvalues in $(1,+\infty)$. Under the weak perturbation characterising *Case (II)* these eigenvalues will (of course) change their values, but the overall structure of the discrete spectrum in the case $\alpha \neq 0$ will remain (more or less) the same, provided that $0 < \beta \ll 1$. In what follows we will let $\lambda_\pm$ denote the values of the two perturbed eigenvalues which are less than unity. The structure of the perturbed spectrum will be discussed by considering separately whether the eigenvalues are either in $(0,1)$ or in $(1,+\infty)$.

5.1 The eigenvalues $\lambda < 1$

We start by introducing the re-scaled variable $\zeta > 0$ given by

$$y = -1 + \beta\zeta\,, \qquad \text{with} \qquad \zeta = \mathcal{O}(1)\,,$$

and then look for solutions of (2.8)-(2.9) in the form

$$f = g_0(\zeta) + \beta^2 g_1(\zeta) + \beta^3 g_2(\zeta) + \dots\,, \tag{5.1a}$$

$$\lambda_* - \lambda = \Delta_1\beta^2 + \Delta_2\beta^3 + \dots\,. \tag{5.1b}$$

In these expansions λ_* is the same as the one defined in (3.6), while the functions $g_j \equiv g_j(\zeta)$ and the coefficients Δ_j $(j = 1, 2, \dots)$ are found by following the usual routine. The situation of interest here is reduced to sequentially solving the following differential equations

$$\mathcal{L}[g_j] \equiv \frac{d^4 g_j}{d\zeta^4} - 2\frac{d^2 g_j}{d\zeta^2} + (1 - \lambda_*)g_j = \mathcal{P}_j\,, \qquad (j = 0, 1, \dots)\,, \tag{5.2}$$

where

$$\mathcal{P}_0 \equiv 0\,, \qquad \mathcal{P}_1 \equiv -(\Delta_1 - \alpha_0)g_0\,, \qquad \mathcal{P}_2 \equiv -(\Delta_2 + \alpha_0)g_0\,, \dots\,.$$

The solutions of (5.2) will be subject to the boundary conditions that follow from (2.9) together with suitable decay properties for g_j and their derivatives as $\zeta \to +\infty$.

The leading-order problem ($j = 0$ in (5.2)) does not yield any new information according to the discussion of λ_* in §3. The next two equations (corresponding to $j = 1$ and $j = 2$, respectively) are both inhomogeneous and require the application of a suitable solvability condition. We note that the leading-order problem is in fact self-adjoint. Thus, the required solvability conditions will be obtained by multiplying the corresponding equations by g_0 and then integrating between $\zeta = 0$ and $\zeta = +\infty$. A direct consequence of this simple argument is that $\Delta_1 = \alpha_0$ and $\Delta_2 = -\alpha_0$, so

$$\lambda_- = \lambda_* - \alpha_0\beta^2 + \alpha_0\beta^3 + \dots\,. \tag{5.3}$$

By considering the boundary layer variable $\xi = \mathcal{O}(1)$ with $y = 1 - \beta\xi$, we find in a similar way that

$$\lambda_+ = \lambda_* + \alpha_0\beta^2 - \alpha_0\beta^3 + \dots\,. \tag{5.4}$$

Comparisons between the predictions of the last two formulae and the results in Table 2 are recorded in Table 3; we note that $\lambda^{(1)} \simeq \lambda_-$ and $\lambda^{(2)} \simeq \lambda_+$ as β decreases.

5.2 The eigenvalues $\lambda > 1$

We look for an outer-type solution of (2.8) with an ansatz of the form

$$f = f_{\text{out}} \equiv G_0(y) + \beta G_1(y) + \beta^2 G_2(y) + \dots\,, \tag{5.5a}$$

$$\lambda = \Lambda_0 + \Lambda_1\beta^2 + \Lambda_2\beta^3 + \dots\,, \tag{5.5b}$$

where the functions G_j and the coefficients Λ_j $(j = 0, 1, 2, \dots)$ will be determined sequentially as explained next.

Table 3: Comparison of the predictions (5.3) and (5.4) with the numerical eigenvalues for *Case (II)* when $\eta = 3\beta^2\varepsilon^2 \simeq \mathcal{O}(\beta^2\varepsilon^2)$ and $\nu = 0.3$; $\lambda^{(j)}$ $(j = 1, 2)$ represent the smallest and the second smallest eigenvalues of the bifurcation problem (2.8)-(2.9).

β	$\lambda^{(1)}$	$\lambda^{(2)}$	λ_-	λ_+
0.05	0.991618867	1.003907307	0.989083235	1.003333235
0.03	0.994267417	0.998491465	0.993589235	0.998827235
0.02	0.995260774	0.997175205	0.995032235	0.997384235
0.01	0.995941831	0.996474357	0.995911235	0.996505235
0.006	0.996107555	0.996308940	0.996100883	0.996315587
0.003	0.996182154	0.996234324	0.996181316	0.996235154

Substituting (5.5) in (2.8) gives $\Lambda_0 = 1$ and Λ_1 is then determined from a reduced second-order boundary-value problem,

$$G_0'' - \frac{1}{2}(\alpha_0 y - \Lambda_1)G_0 = 0\,, \qquad G_0(\pm 1) = 0\,, \tag{5.6}$$

where the 'dash' indicates differentiation with respect to $y \in [-1, 1]$. In deriving the boundary constraints for the differential equation in (5.6) it was assumed that $\nu \neq 0$. One can solve (5.6) using standard numerical methods or, alternatively, it can be reduced to a standard Airy equation as in §4; we will follow the second approach. To this end, let $\omega_0 := (\alpha_0/2)^{1/3}$ and set $z := \omega_0 y - \Lambda_1/(2\omega_0^2)$. With this change of variable the solution of the differential equation in (5.6) is $G_0 = d_1\mathrm{Ai}(z) + d_2\mathrm{Bi}(z)$ for arbitrary d_1, $d_2 \in \mathbb{R}$; here, 'Bi' represents the Airy function of the second kind (e.g., [31, 32]). Enforcing the boundary conditions on the above expression of G_0 leads to the determinantal equation

$$\mathrm{Ai}(z^+)\mathrm{Bi}(z^-) - \mathrm{Ai}(z^-)\mathrm{Bi}(z^+) = 0\,, \qquad z^\pm := \pm\omega_0 - \frac{\Lambda_1}{2\omega_0^2}\,, \tag{5.7}$$

whereby Λ_1 will become available once β and $\widetilde{\alpha}$ have been specified. Regarded as a function of Λ_1, the expression on the left side of the equality sign in (5.7) is oscillatory and has an infinite number of roots; the smallest positive root is the one of interest in the present context.

The next correction term in the approximation of the eigenvalue λ is obtained from the solution of an inhomogeneous differential equation

$$G_1'' - \frac{1}{2}(\alpha_0 y - \Lambda_1)G_1 = -\frac{1}{2}\Lambda_2 G_0\,, \tag{5.8}$$

but the corresponding boundary constraints on G_1 will be dictated by additional boundary layers at $y = \pm 1$ (as seen in §3). Since the differential operator on the left-hand side in (5.8) is self-adjoint, the solvability condition for G_1 is obtained by multiplying the equation by G_0 and then integrating over $[-1, +1]$. Integration by parts in conjunction with the boundary constraints on G_1 yields

$$-\frac{1}{2}\Lambda_2 \int_{-1}^{+1} G_0^2\,\mathrm{d}y = [\![G_0 G_1' - G_0' G_1]\!]_{-1}^{+1}\,, \tag{5.9}$$

where we have used the notation $[\![\varphi]\!]_{-1}^{+1} := \varphi(+1) - \varphi(-1)$, for $\varphi \equiv \varphi(y)$ an arbitrary function. In order to benefit from the formula (5.9) stated above, we still need full knowledge of the boundary terms that appear there. The first term in the right-hand side bracket will be zero owing to (5.6), while the values $G_0'(\pm 1)$ are also available from the numerical solution of the same problem. However, for $G_1(\pm 1)$ we must turn to a local boundary-layer analysis of the regions adjacent to the locations $y = \pm 1$. The leading-order analysis needed for our immediate purposes is identical to what was discussed in §4.2, except that the inner-layer ansatz will be of the form

$$f = f_{\rm inn} \equiv \beta f_0(\overline{Y}) + \beta^2 f_1(\overline{Y}) + \dots\,, \qquad \overline{Y} \equiv \beta^{-1}(1+y)\,.$$

The stated expansion pertains to the left boundary layer ($y = -1$), with a comparable asymptotic structure in place near $y = 1$ (obtained by making the change $\overline{Y} \to \beta^{-1}(1-y)$). The outcome of this elementary analysis is that

$$G_1(\pm 1) \to \pm \frac{(2-\nu)^2}{\nu^2\sqrt{2}} G_0'(\pm 1)\,, \qquad (\nu \neq 0)\,. \tag{5.10}$$

By making use of (5.9) and (5.10), the correction term Λ_2 can then be evaluated numerically. Some illustrative comparisons between the three-term approximation derived above and direct numerical simulations of the main bifurcation problem are included in Table 4.

Table 4: Examples of predictions obtained from formula (5.5b) and the corresponding direct numerical simulations of the eigenproblem (2.8)-(2.9).

β	brute-force numerics	formula (5.5b)
0.01	1.000792504	1.000716826
0.008	1.000460992	1.000429172
0.006	1.000234906	1.000224761
0.003	1.000050571	1.000049947

6 Concluding remarks

In this study, an earlier numerical investigation [10, 11] exploring the divergence-type instabilities of non-uniformly tensioned traveling webs has been augmented with an asymptotic interpretation. Upon introducing a non-dimensional (stretched) *plate parameter*, denoted by $0 < \varepsilon \ll 1$ as defined in (3.1), our work has confirmed that some of the various types of critical eigenmodes identified in the aforementioned references are intimately linked to a couple of asymptotic regimes. We have presented new theoretical evidence suggesting that these regimes are indeed influenced by the degree of non-uniformity in the applied tension relative to the magnitude of the small quantity ε. In the interest of brevity, here the discussion has been confined to isotropic elastic webs. There is no particular difficulty in extending the proposed analysis to orthotropic webs (which would be more realistic for materials like 'paper'); the corresponding equations for such anisotropic configurations, akin to (2.3) and (2.5) in §2, can be found in [11].

Certainly, the selection of the asymptotic parameter β in our analysis deviates from the norm and is rather unorthodox. This choice stems from two primary reasons. Initially, as highlighted earlier (in §2), it was noted that for the plates under consideration, this parameter remained relatively small.

Therefore, our choice can be formally justified in this context. A second and more significant rationale behind formulating the asymptotic analysis in terms of β is linked to the preceding works [10, 11, 33], which we aimed to provide fresh insights into. The concern was that altering the scaling of the original problem would merely result in a more tenuous connection to those studies. In our current asymptotic developments the plate parameter ε does not appear explicitly. We recall that $\widetilde{\alpha}_{\max} = \varepsilon^{-2}$ and $\widetilde{\alpha} = \eta\widetilde{\alpha}_{\max}$, with η being the actual quantity that was varied by the previous authors; β was clearly regarded as being independent of ε. A different interpretation of the problem taken up in this paper has been recently reported elsewhere [41]. We also mention in passing that the two cases (I) and (II) defined in (3.2) do not exhaust all conceivable possibilities. For example, if $\widetilde{\alpha}/\widetilde{\alpha}_{\max} = \mathcal{O}(\varepsilon^2/\beta)$ then the critical eigenmodes will still be localised near the edge $y = -1$, but this time there is just one distinct boundary-layer structure at play. Within that region, the original differential equation (2.8) maintains its order, and the spatially-varying term still remains present, rendering a straightforward closed-form solution unattainable. It can be further shown that the critical eigenvalue admits an approximation of the form $\lambda = \beta^{-1}\lambda_0 + \lambda_1 + \ldots$, in which $\lambda_0 = \mathcal{O}(1)$ is related to $\widetilde{\alpha}$ and $\lambda_1 = \mathcal{O}(1)$ is obtained by solving numerically the aforementioned boundary-layer equation.

The tractability of the model investigated in the foregoing sections is obviously linked to the simplified nature of the stress distribution (2.1) in the pre-buckling range. Such simplifications, based on adopting some form of symmetry for the basic state, are quite common in the literature on elastic stability of plates shells [11, 38], and even in finite elasticity (e.g., see [42]). Some authors (e.g, [43, 44]) have been concerned with more accurate descriptions of the stresses in stretched and axially moving webs. For example Lin and Mote [43] considered the effect of a transverse pressure and showed that this leads to the presence of boundary layers along both the free edges and near the rollers; away from those regions, in the central part of the web, a membrane-like state of stress was found to prevail. The two examples considered in [43] are not especially enlightening, yet transverse pressure gradients arising as a result of the interaction between the web and the surrounding air are likely to have a destabilising influence on a rapidly moving plate-like structure (e.g., see [45] and the references therein); this effect should be incorporated in a more realistic model of the situation explored herein.

Some remarks regarding the separation of variables in (2.7) are worth spelling out. That form of solution was predicated on the *a priori* assumption that the axial deformation of the web is a half-sine shape. In general, there is no quarantee that such particular solutions will represent minimum energy configurations for the buckled web (a moot point in the work of our predecessors). We have carried out additional numerical work in which we explored the more general expression $w(x, y) = f(y)\sin(m\pi x)$, where $m \in \mathbb{N}$ represents the so-called *axial mode number*, a quantity that has to be determined as part of the solution as explained, for instance, in [5, 14, 29]. For the physical/geometrical parameter values used by Banichuk *et al.* [10, 11], the critical mode number is indeed $m = 1$. This remains true if $\varepsilon > 0$ is fixed and $\beta \to 0^+$, so the simplified form of solution (2.7) does not affect the findings of the current asymptotic study. However, even for the values chosen in the references just cited, if $\widetilde{\alpha}/\widetilde{\alpha}_{\max} \simeq 0.75$ (a value beyond the scope of the two cases explored in this paper), the critical mode number is $m = 2$. As shown in the forthcoming work [41], if $\beta > 0$ is fixed but $\varepsilon \to 0^+$ then the mode number associated with the smallest eigenvalue can be arbitrarily large – at least in some (fairly general) circumstances.

Throughout this study, we have focused solely on divergence-type instabilities, directing our interest towards web- rather than strip-like planar geometries. Of course, dynamic instabilities (i.e., flutter) might become important when the aspect-ratio parameter $\beta \gg 1$. However, this situation cannot be handled by recourse to the simple-minded mode reduction employed in (2.7); as a result, the solution strategy adopted in this study has limited applicability in that context. The reader is referred to the work of Lin [21], who carried out a partial numerical investigation of both divergence- and flutter-type instabilities in uniformly tensioned and axially moving thin elastic strips. An extension of that work to the case of non-uniform tension will be reported elsewhere.

Acknowledgement
The referees are thanked for their comments that have helped improve the presentation of the paper.

References

[1] Jacques, N., Potier-Ferry, M.: On mode localisation in tensile plate buckling. Comptes Rendus Mécanique **333**, 804–809 (2005)

[2] Puntel, E., Deseri, L., Fried, E.: Wrinkling of a stretched thin sheet. Journal of Elasticity **105**, 137–170 (2011)

[3] Nayyar, V., Ravi-Chandar, K., Huang, R.: Stretch-induced stress patterns and wrinkles in hyperelastic sheets. International Journalof Solids and Structures **48**, 3471–3483 (2011)

[4] Xin, M., Davidovitch, B.: Stretching Hookean ribbons II: from buckling instability to far-from threshold wrinkle pattern. European Physics Journal E **44:94**, (2021)

[5] Coman, C.D.: Edge-wave buckling of rolled elastic strips. Acta Mechanica **211**, 101–113 (2010)

[6] Coman, C.D.: The asymptotic limit of an eigenvalue problem related to buckling of rolled elastic strips. Mechanics Research Communications **36**, 826–832 (2009)

[7] Fisher, F.D., Rammerstorfer, F.G., Friedl, N., Wisser, W.: Buckling phenomena related to rolling and levelling of sheet metal. International Journal of Mechanical Sciences **42**, 1887–1910 (2000)

[8] Shelton, J.J., Reid, K.N.: Lateral dynamics of an idealized moving web. ASME Journal of Dynamic Systems, Measurement, and Control **93**, 187–192 (1971)

[9] Lakshmikumaran, A.V., Wickert, J.A.: Edge buckling of imperfectly guided webs. ASME Journal of Applied Mechanics **120**, 346–352 (1998)

[10] Banichuk, N., Jeronen, J., Neittaanmäki, P., Saksa, T., Tuovinen, T.: Theoretical study on travelling web dynamics and instability under non-homogeneous tension. International Journal of Mechanical Sciences **66**, 132–140 (2013)

[11] Banichuk, N., Barsuk, A., Jeronen, J., Tuovinen, T., Neittaanmäki, P.: Stability of Axially Moving Materials. Springer, Dordrecht (2020)

[12] Mockensturm, E.M., Mote, C.D.: Free response of twisted plates with fixed support separation. ASME Journal of Vibration and Acoustics **123**, 175–180 (2001)

[13] Mockensturm, E.M.: The elastic stability of twisted plates. ASME Journal of Applied Mechanics **68**, 561–567 (2001)

[14] Coman, C.D., Bassom, A.P.: An asymptotic description of the elastic instability of twisted thin elastic plates. Acta Mechanica **200**, 59–68 (2008)

[15] Leipholz, H.: Stability of Elastic Systems. Noordhoff International Publishing, Leyden, The Netherlands (1980)

[16] Nguyen, Q.S.: Stability and Nonlinear Mechanics. John Wiley & Sons, Chichester, UK (2000)

[17] Luongo, A., Feretti, M., Di Nino, S.: Stability and Bifurcation of Structures. Springer, Dordrecht (2023)

[18] Mote, C.D.: Dynamic stability of axially moving materials. Shock and Vibration Digest **4**, 2–11 (1972)

[19] Wickert, J.A., Mote, C.D.: Current research on the vibration and stability of axially moving materials. Shock and Vibration Digest **20**, 3–13 (1988)

[20] Ulsoy, A.G., Mote, C.D.: Vibration of wide band saw blades. ASME Journal of Engineering for Industry **104**, 71–78 (1982)

[21] Lin, C.C.: Stability and vibration characteristics of axially moving plates. International Journal of Solids and Structures **34**, 3179–3190 (1997)

[22] Scheidl, J., Vetyukov, Y.: Review and perspectives in applied mechanics of axially moving flexible structures. Acta Mechanica **234**, 1331–1364 (2023)

[23] Pham, P-T., Hong, K-S.: Dynamic models of axially moving systems: A review. Nonlinear Dynamics **100**, 315–349 (2020)

[24] Zhu, H., Zhu, W.D., Fan, W.: Dynamic modeling, simulation and experiment of power transmission belt drives: A systematic review. Journal of Sound and Vibration **491**, 115759 (2021)

[25] Marynowski, K., Kapitaniak, T.: Dynamics of axially moving continua. International Journal of Mechanical Sciences **81**, 26–41 (2014)

[26] Hong, C.D., Chen, L-Q., Pham, P-T., Yang, X-D.: Control of Axially Moving Systems. Springer, Singapore (2022)

[27] Veits, V.L., Beilin, I.Sh., Merkin, V.M.: Free vibrations of an unevenly tensioned tape. Soviet Applied Mechanics **26**, 378–385 (1990)

[28] Lin, C.C., Mote, C.D.: The wrinkling of rectangular webs under nonlinearly distributed edge loading. Journal of Applied Mechanics **63**, 655–659 (1996)

[29] Coman, C.D., Bassom, A.P.: Higher-order asymptotics for pre-stressed thin films under in-plane bending. Journal of Engineering Mathematics **63**, 327–338 (2009)

[30] Coman, C.D.: Edge-buckling in stretched thin films under in-plane bending. Zeitschrift für Angewandte Mathematik und Physik **58**, 510–525 (2007)

[31] Andrews, L.C.: Special Functions of Mathematics For Engineers, McGraw-Hill Inc., New York (1992).

[32] Lebedev, N.N.: Special Functions and Their Applications, Dover Publications Inc., New York (1972).

[33] Banichuk, N., Jeronen, J., Neittaanmäki, P., Tuovinen, T.: On the instability of an axially moving elastic plate. International Journal of Solids and Structures **47**, 91–99 (2010)

[34] Timoshenko, S., Goodier, J.N.: Theory of Elasticity (Third Ed.). McGraw-Hill Book Company, New York (1970)

[35] Coman, C.D., Bassom, A.P.: On the wrinkling of a pres-stressed annular thin film in tension. J. Mech. Phys. Solids **55**, 1601–1617 (2007)

[36] Coman, C.D., Haughton, D.M.: Localized wrinkling instabilities in radially stretched annular thin films. Acta Mechanica **185**, 179–200 (2006)

[37] Coman, C.D.: Continuum Mechanics and Linear Elasticity. Springer, Dordrecht (2020)

[38] Brush, Don O., Almroth, Bo O.: Buckling of Bars, Plates and Shells. McGraw-Hill Book Company, New York (1975)

[39] Niordson, F.I..: Shell Theory. North-Holland, Amsterdam (1985)

[40] Ventsel, E., Krauthammer, T.: Thin Plates and Shells: Theory, Analysis, and Applications. Marcel Dekker, Inc., New York (2001)

[41] Coman, C.D.: On the partial wrinkling of imperfectly guided webs. Mechanics Research Communications (submitted for publication)

[42] Ogden, R.W.: Non-Linear Elastic Deformations. Dover Publications, Mineola (1997)

[43] Lin, C.C., Mote, C.D.: Equilibrium displacement and stress distribution in a two-dimensional, axially moving web under transverse loading. Journal of Applied Mechanics **62**, 722–779 (1995)

[44] Luo, A.C.J., Hamidzadeh, H.R.: Equilibrium and buckling stability for axially traveling plates. Communications in Nonlinear Science and Numerical Simulation **9**, 343–360 (2004)

[45] Algazin, S.D., Kijko, I.A.: Aeroelastic Vibrations and Stability of Plates and Shells. De Gruyter, Berlin (2015)